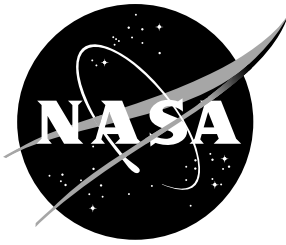


NASA Technical Memorandum 110272



Cryogenic Tunnel Pressure Measurements on a Supercritical Airfoil for Several Shock Buffet Conditions

Robert E. Bartels and John W. Edwards
Langley Research Center, Hampton, Virginia

September 1997

National Aeronautics and
Space Administration
Langley Research Center
Hampton, Virginia 23681-0001

Cryogenic Tunnel Pressure Measurements on a Supercritical Airfoil for Several Shock Buffet Conditions

Robert E. Bartels and John W. Edwards

NASA Langley Research Center, Hampton, Virginia 23681-0001.

Summary

Steady and unsteady experimental data are presented for several fixed geometry conditions from a test in the NASA Langley 0.3-Meter Transonic Cryogenic Tunnel. The purpose of this test was to obtain unsteady data for transonic conditions on a fixed and pitching supercritical airfoil at high Reynolds numbers. Data and brief analyses for several of the fixed geometry test conditions will be presented here. These are at Reynolds numbers from 6×10^6 to 35×10^6 based on chord length, and span a limited range of Mach numbers and angles of attack just below and at the onset of shock buffet. Reynolds scaling effects appear in both the steady pressure data and in the onset of shock buffet at Reynolds numbers of 15×10^6 and 30×10^6 per chord length.

Introduction

Frequently the objective in two dimensional wind tunnel experiments involving conventional and supercritical airfoils is to obtain data for steady or pitching airfoils. Shock buffet is seen as a limit on the range of useful data. Thus, it is valuable to be able to predict the onset of this behavior. The purpose of this paper is to make available two-dimensional wind tunnel test data of the SC(2)-0714 airfoil that reveal shock buffet behavior.

Onset of shock buffet for a conventional airfoil was studied extensively in reference 1. Experimental studies through the Mach number range at and beyond buffet onset for several supercritical airfoils confirms that

these airfoils can also experience shock buffet (refs. 2 and 3). Currently there is no study of such issues as Reynolds scaling of this phenomenon at realistic flight Reynolds numbers. In this regime transition can be expected to occur at or near the leading edge, and Reynolds number effects would usually be due to scaling of the turbulent boundary layer. Although Reynolds number scaling effects studied in a wind tunnel context is a complicated matter, its relation to unsteady transonic conditions is a subject worthy of attention. The present paper is not a comprehensive study of this problem but is a presentation of selected data from a high Reynolds number study made in the 0.3 Meter Transonic Cryogenic Tunnel at the NASA Langley Research Center. There are several test conditions out of that study that are of interest in the present context.

That test and the resulting data were discussed in a previous report (ref. 4). The purpose of that report was to provide unsteady pressure data for comparison with CFD codes for the airfoil undergoing harmonic pitching oscillations for Reynolds numbers ranging from 6 to 35×10^6 based on chord length. Baseline data were also obtained, with the model at a fixed angle, for all of the Mach number, Reynolds number, and angle combinations tested. Several of these steady test conditions exhibited shock buffet. Since the SC(2)-0714 represents a modern airfoil type for transonic flight, it is desirable to make this data available for comparison with computations as well. The present paper presents data for several conditions near shock buffet onset of the SC(2)-0714 supercritical airfoil at several high Reynolds numbers.

Test Setup

Only a few details pertaining to the test procedure will be presented here. A more complete discussion can be found in reference 4. Although wind tunnel turbulence has been measured for other tests conducted in this tunnel, (ref. 5) it was not measured during this test. Floor and ceiling walls were slotted. Although the tunnel is capable of side wall suction it was not used in the test presently being discussed. Corrections for side wall boundary layer blockage can be found in reference 6. Angle of attack corrections to account for downwash caused by the slotted floor and ceiling walls can be found in reference 7. Neither of these corrections has been applied to the present data.

The airfoil had a 6 inch chord and an 8 inch span. The surface was polished and no transition strips were used. A total of forty three unsteady pressure transducers were mounted internally and distributed over both surfaces in three spanwise rows. The transducer configuration can be found in reference 4 and is also reproduced in Figure 1. Pressure data from these transducers was recorded on analog tape records.

Following the test these analog tape records were converted to digital calibrated data files. For the cases presented herein, digitization was at 5000 samples per second. At this time, a slight time misalignment between the two sets of files was discovered. For the cases presented in this report, the time misalignments range from 0.001 to 0.040 seconds. Due to this misalignment, time correlation studies of variables recorded on the different units are not possible. However, it is possible to make a spectral analysis of the individual unsteady pressures. This has been done with a discrete Fourier transform analysis package assembled by the authors, based on the fast Fourier transform (FFT) subroutines found in reference 8. Spectral analysis of these data sets was made with this package using block sizes of 16384. Smoothing of the transforms was accomplished using 75% overlap block averaging and a low frequency window function.

Pressure data are available for the complete set of data points shown in Table 1. The Table gives the identifying Run and Data Point numbers for these fixed geometry conditions. The experimental Mach number, angles and Reynolds number are included. The seven cases which are highlighted with shading are discussed in the remainder of this report. Figure 2 indicates the relationship of these seven cases to the experimental shock buffet onset boundary. The experimental data was obtained with 0.5 degree angle of attack increments and the shaded region in the figure defines the range within which shock buffet onset was observed. Figure 3 presents the chordwise distributions of the mean of the pressure coefficients for Cases 1-3 where $M_{exp} = 0.72$ and $\alpha_{exp} = 2.5$ degrees. The data for Reynolds numbers of 15 and 30 million are in good agreement, while at a Reynolds number of 6 million the shock is significantly forward.

The pressure coefficient time history records were analyzed with a fast Fourier transform program. Figures 4-6 present, for Cases 1-3, the chordwise distribution of the resulting modulus squared of the unsteady component of the upper surface pressure coefficient versus frequency for each chordwise pressure sensor location from $x/c = 0.42$ to 0.95. For all three Reynolds numbers, significant amplitudes are only seen in the vicinity of the shock. Note that the majority of the unsteadiness is at low frequency although low levels of unsteadiness extend in a broad band pattern up to at least several hundred Hertz. This is consistent with intermittent jumps in shock location across one or two pressure sensors, a feature that can also be observed in the pressure traces for another condition shown in reference 4. The most notable feature, however, is the variation in shock location with Reynolds number seen in the chordwise distributions of mean pressure coefficient shown in Figure 3.

Figure 7 shows the chordwise distribution of the mean of the pressure coefficients for Cases 4 and 6 where $M_{exp} = 0.74$ and $\alpha_{exp} = 2.0$ degrees. Here again there is little difference in pressure levels or shock locations for Reynolds numbers of 15 and 30

million, while the shock location has moved rearward just beyond $x/c = 0.60$. The modulus squared of the pressure coefficient versus frequency and chordwise location is shown in Figures 8 and 9 for these two cases. As for Cases 1-3, significant levels are seen only in the vicinity of the shock. Again, low frequency oscillations (0-10 Hz) predominate. At $x/c = 0.62$ and 0.66 low amplitude levels are seen for frequencies up to about 150 Hz and these levels have increased from corresponding levels seen in Figures 4-6.

Reference 4 reports episodes of isolated shock motion near several transducers at $M_{exp} = 0.72$, $\alpha_{exp} = 2.0^\circ$ and $Re = 35 \times 10^6$. Although not discussed in that report, nearly continuous shock buffet occurs at $M_{exp} = 0.74$ and $\alpha_{exp} = 3.0^\circ$ for Reynolds numbers of 15×10^6 and 30×10^6 . Thus, for $M_{exp} = 0.74$, shock buffet evidently develops in the range $\alpha_{exp} = 2.0 - 3.0$ degrees. The precise location is unknown since only one intermediate data point between 2.0 and 3.0 degrees at $Re = 30 \times 10^6$ was taken. Figure 10 shows the chordwise distributions of the mean of the pressure coefficients for Cases 5 and 7 where $M_{exp} = 0.74$ and $\alpha_{exp} = 3.0$ degrees. Now the pressure gradients through the shock are lower than those shown in Figures 3 and 7 and the shock location has moved forward to slightly less than $x/c = 0.60$. This reversal of the aftwards motion of the shock with increasing angle of attack, sometimes referred to as "shock stall", is associated with separation onset. The lowering of the mean pressure gradient at the shock is associated with the onset of large scale shock motions.

These motions are evident in the chordwise distribution of the modulus squared of the unsteady upper surface pressure coefficient versus frequency and chordwise location for Cases 5 and 7 shown in Figures 11 and 12. At $Re = 15 \times 10^6$, Figure 11, a prominent spectral peak near 70 Hz is seen from $x/c = 0.46$ to 0.62 with the largest amplitude at $x/c = 0.54$. Although reduced in amplitude, this feature is also observed at all stations downstream. The same shock oscillation behavior is seen in Figure 12, where $Re = 30 \times 10^6$. The reduced frequencies ($k_{exp} = 2\pi f(c/2)/U$) of the fundamental shock oscillation modes, as shown in

the modulus squared of the pressure coefficients versus frequency in Figure 13 and versus chordwise location in Figure 14, are in the range $k_{exp} = 0.19 - 0.21$ at $Re = 15 \times 10^6$ and $k_{exp} = 0.20 - 0.23$ at $Re = 30 \times 10^6$. There appear to be higher harmonics associated with the shock oscillation at both Reynolds numbers as evidenced by the small peaks at higher frequencies in Figures 11-14. Also note that the low frequency peak seen in the "steady" cases is largely absent from the buffet cases.

By comparing Figures 11 and 12 with Figures 8 and 9 it is clear that shock buffet does not occur at $\alpha_{exp} = 2.0$ degrees at either Reynolds number, but does occur at both Reynolds numbers at $\alpha_{exp} = 3.0$ degrees. The intensity of the shock buffet is somewhat lower at the higher Reynolds number. The chordwise distributions of the modulus squared of the unsteady pressure coefficient at frequencies near the fundamental shock oscillation mode show that the region in which the shock moves shifts approximately 6 percent aft in going from a Reynolds number of 15×10^6 to 30×10^6 . This shift in the location of the shock motion with Reynolds number is consistent with the shift observed in reference 4 for pitching airfoils and in the Reynolds number effect on steady shock location for the supercritical airfoil SC(2)-0712A, also tested in this tunnel (ref. 5).

Finally, a notable Reynolds scale effect is observed in the mean of the unsteady trailing edge pressures shown in Figure 10 that is largely absent from the steady trailing edge pressures shown in Figure 7. A common use of steady pressure measurements in the vicinity of trailing edges is the inference of buffet onset when this pressure fails to recover to a level higher than some small negative value. Clearly, use of this criteria for the two cases in Figure 10 is inappropriate since in both cases large shock oscillations are seen while the data in the figure indicates recovery to positive pressure, at least for the higher Reynolds number case. The Reynolds scale effect seen for $x/c = 0.95$ would appear to have implications for this use of trailing edge "divergence" of pressure as an indicator of buffet onset.

Concluding Remarks

Experimental data has been analyzed from a previous test of a 14 percent thick supercritical low aspect ratio wing section model at Reynolds numbers from 6×10^6 to 30×10^6 at transonic Mach numbers. Although three dimensional effects can be expected to be significant for a model of low aspect ratio, no attempt has been made to quantify these effects. An analysis that assumes the flow to be symmetric about the wing mid span has been performed of the pressure data taken along two chordwise rows located near the mid span. Steady conditions have shown from moderate to strong low frequency unsteadiness localized near the shock. In contrast, shock buffet cases exhibit large scale shock motion and flow unsteadiness which encompasses the region from the shock to the trailing edge. They also exhibit a significant reduction in the mean pressure gradient through the shock. A Reynolds scale effect has been observed in the somewhat reduced intensity of the shock buffet at the higher Reynolds number. Mean pressures at the trailing edge for shock buffet cases at several Reynolds numbers also show a Reynolds scaling of the turbulent boundary layer. While trailing edge pressure divergence is seen in the lower Reynolds number buffet condition it is not evident in the buffet data at the higher Reynolds number. Further investigation of the effect of side wall boundary layer interference, variation in transition location, fixed versus free transition and the interplay between these and a Reynolds scaling of the turbulent boundary layer needs to be made.

References

- [1] McDevitt, John B.; and Okuno, Arthur F.: Static and Dynamic Pressure Measurements on a NACA 0012 Airfoil in the Ames High Reynolds Number Facility. NASA TP-2485, June 1985.
- [2] Roos, Frederick W.: Some Features of the Unsteady Pressure Field in Transonic Airfoil Buffeting. *Journal of Aircraft*, Vol. 17, No. 11, November 1980, pp. 781-788.
- [3] Roos, F. W.: Surface Pressure and Wake Flow Fluctuations in a Supercritical Airfoil Flowfield. AIAA-75-0066, 1975.
- [4] Hess, Robert W.; Seidel, David A.; Igoe, William B; and Lawing, Pierce L.: Highlights of Unsteady Pressure Tests on a 14 Percent Supercritical Airfoil at High Reynolds Number, Transonic Condition. NASA TM-89080, January 1987.
- [5] Ray, E. J.: A Review of Reynolds Number Studies Conducted in the Langley 0.3-m Transonic Cryogenic Tunnel. AIAA-82-0941, June 1982.
- [6] Jenkins, Renaldo V., Adcock, Jerry B.: Tables for Correcting Airfoil Data Obtained in the Langley 0.3-Meter Transonic Cryogenic Tunnel for Sidewall Boundary Layer Effects. NASA TM-87723, June 1986.
- [7] Barnwell, Richard W.: Design and Performance Evaluation of Slotted Walls for Two-Dimensional Wind Tunnels. NASA TM-78648, February 1978.
- [8] Walker, James S.: *Studies in Advanced Mathematics, Fast Fourier Transforms*. CRC Press, Boca Raton, 1991.

Table 1: SC(2)-0714 Fixed Geometry Conditions

Run	Data Point	M_{exp}	$Re (X10^{-6})$	α_{exp} (Deg.)	Case
8	201A	0.65	30	0.0	
↓	208	↓	↓	1.0	
↓	215A	↓	↓	2.0	
21	530	0.70	15	-2.0	
↓	541	↓	↓	-1.0	
↓	552	↓	↓	0.0	
22	563A	↓	↓	1.0	
23	575	↓	↓	2.0	
↓	589	↓	↓	3.0	
6	98A	↓	30	-2.0	
↓	107A	↓	↓	-1.0	
↓	123A	↓	↓	1.0	
33	886	↓	↓	2.0	
6	139	↓	↓	2.5	
33	903	↓	↓	3.0	
14	372	↓	35	-2.5	
↓	365A	↓	↓	-2.0	
↓	362	↓	↓	-1.5	
↓	356	↓	↓	-1.0	
↓	334A	↓	↓	0.0	
↓	341	↓	↓	1.0	
↓	349A	↓	↓	2.0	
↓	355	↓	↓	2.5	
16	416A	0.72	6	-2.5	
↓	417	↓	↓	-2.0	
↓	429	↓	↓	-1.0	
↓	442	↓	↓	0.0	
4	52A	↓	↓	1.0	
16	452	↓	↓	2.0	
4	65	↓	↓	2.5	1
18	462A	↓	10	-2.5	
↓	463A	↓	↓	-2.0	
↓	475	↓	↓	-1.0	
19	487A	↓	↓	0.0	
20	501B	↓	↓	1.0	
↓	513	↓	↓	2.0	

Table 1: (Concluded)

Run	Data Point	M_{exp}	$Re(X10^{-6})$	α_{exp} (Deg.)	Case
27	661A	0.72	15	-2.0	
↓	677	↓	↓	-1.0	
↓	693	↓	↓	0.0	
28	709A	↓	↓	1.	
29	726	↓	↓	2.0	
10	276	↓	↓	2.5	2
2		↓	↓		
15	375A	↓	20	-2.5	
↓	376	↓	↓	-2.0	
↓	384	↓	↓	-1.0	
↓	391	↓	↓	0.0	
↓	399A	↓	↓	1.0	
↓	406	↓	↓	2.0	
↓	412	↓	↓	2.5	
30	742	↓	↓	-2.0	
↓	760	↓	↓	-1.0	
5	81A	↓	↓	1.0	
↓	88A	↓	↓	2.0	
↓	94	↓	↓	2.5	3
9	229A	↓	35	-2.0	
12	302	↓	↓	-1.0	
13	311	↓	↓	0.0	
↓	318	↓	↓	1.0	
↓	325	↓	↓	2.0	
24	593A	0.74	15	-2.0	
↓	604	↓	↓	-1.0	
25	615A	↓	↓	0.0	
↓	630	↓	↓	1.0	
26	644A	↓	↓	2.0	4
↓	659	↓	↓	3.0	5
7	143A	↓	30	-2.0	
34	907B	↓	↓	-1.0	
↓	922	↓	↓	0.0	
↓	937	↓	↓	1.0	
35	953	↓	↓	2.0	6
↓	972	↓	↓	2.5	
↓	973	↓	↓	3.0	7

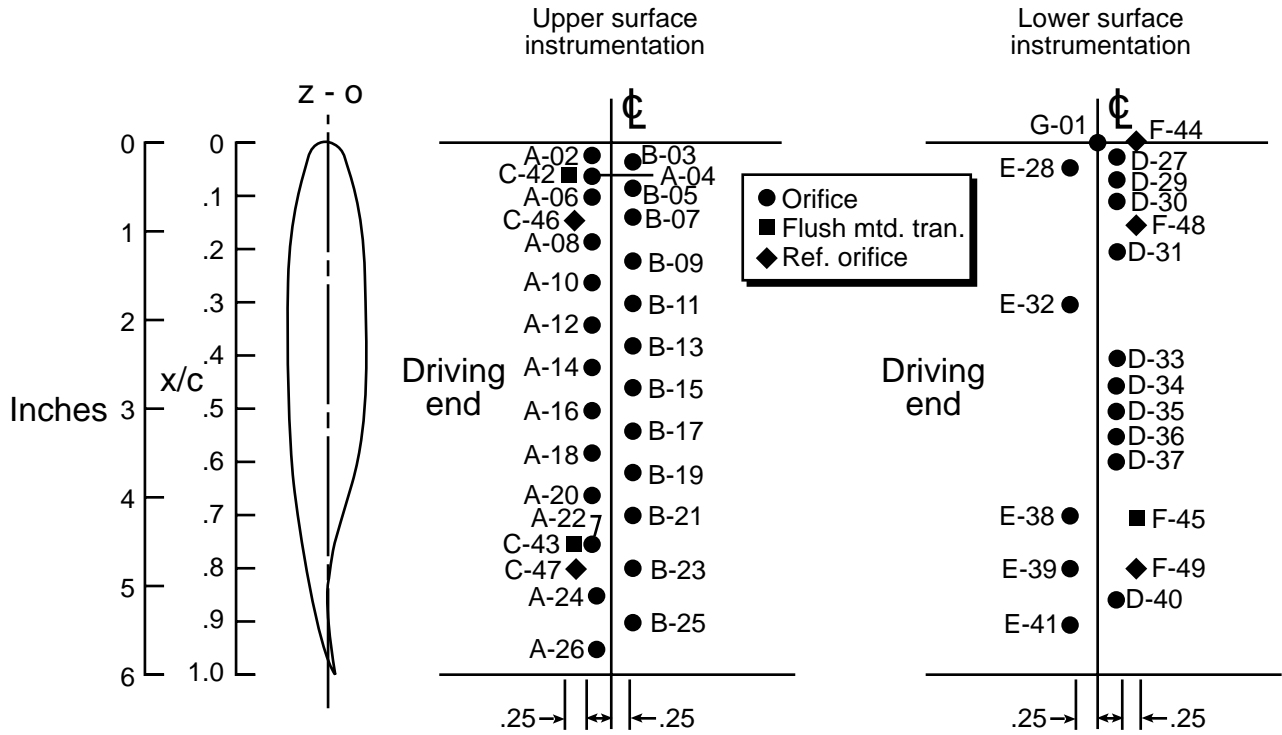


Figure 1. SC(2)-0714 airfoil and pressure transducer geometry.

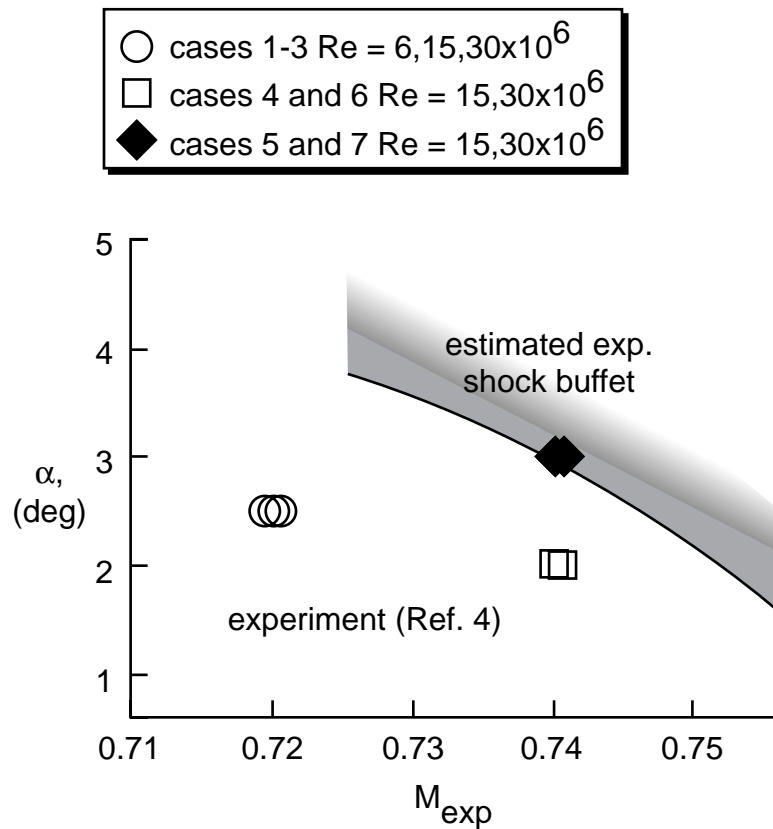


Figure 2. SC(2)-0714 airfoil steady and unsteady cases, experiment.

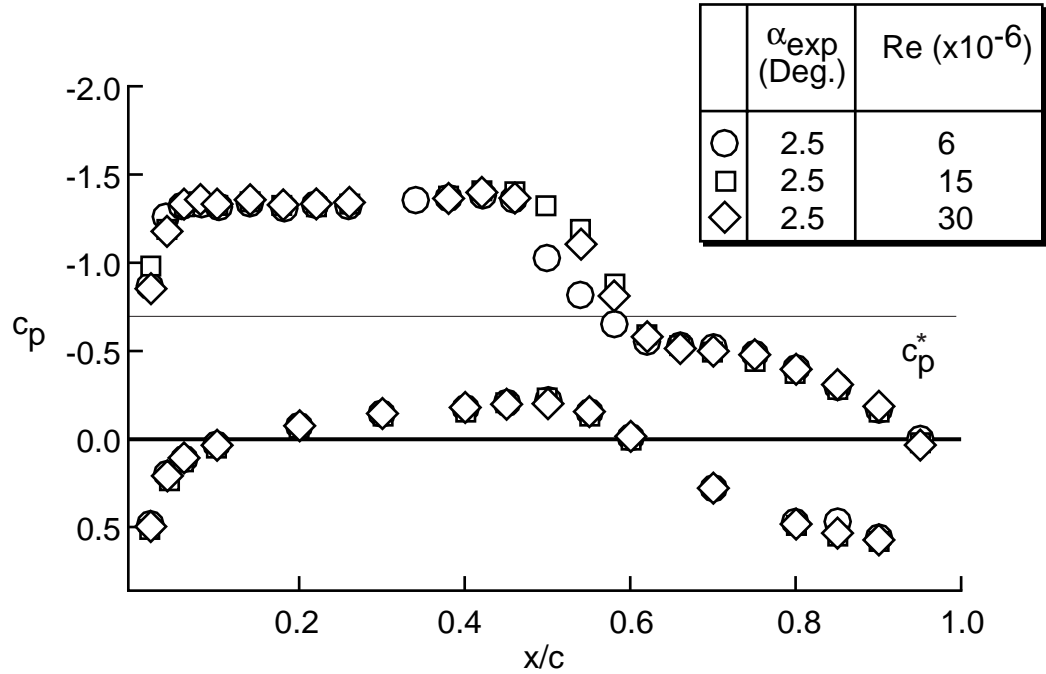


Figure 3. Chordwise distribution of mean pressure coefficient ,
Cases 1-3, $M_{exp} = 0.72$.

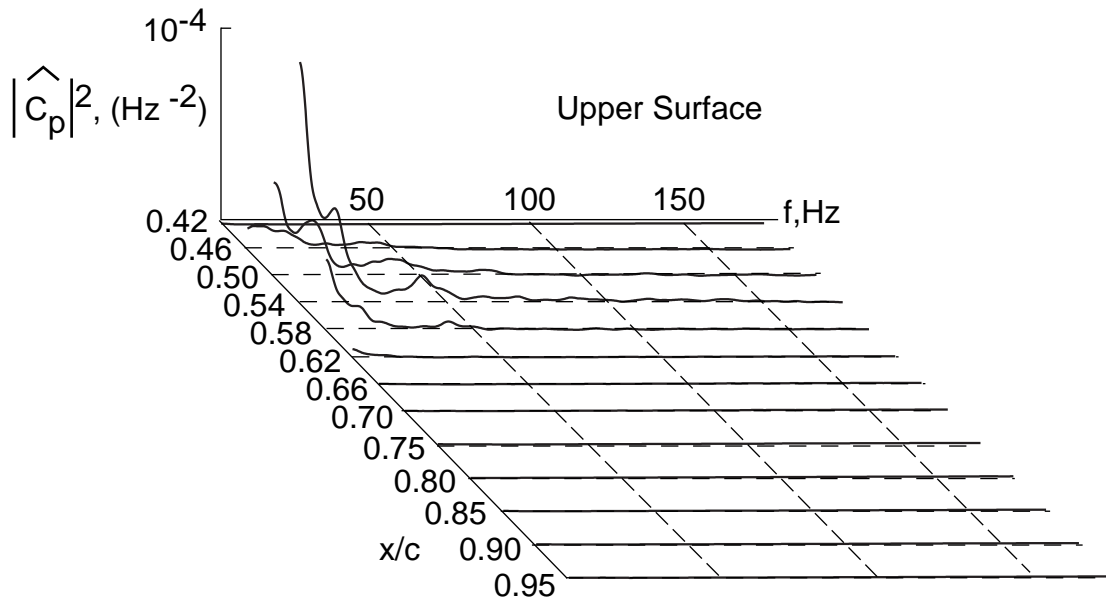


Figure 4. Chordwise distribution of unsteady airfoil pressure coefficient modulus squared,
Case 1, $Re = 6 \times 10^6$.

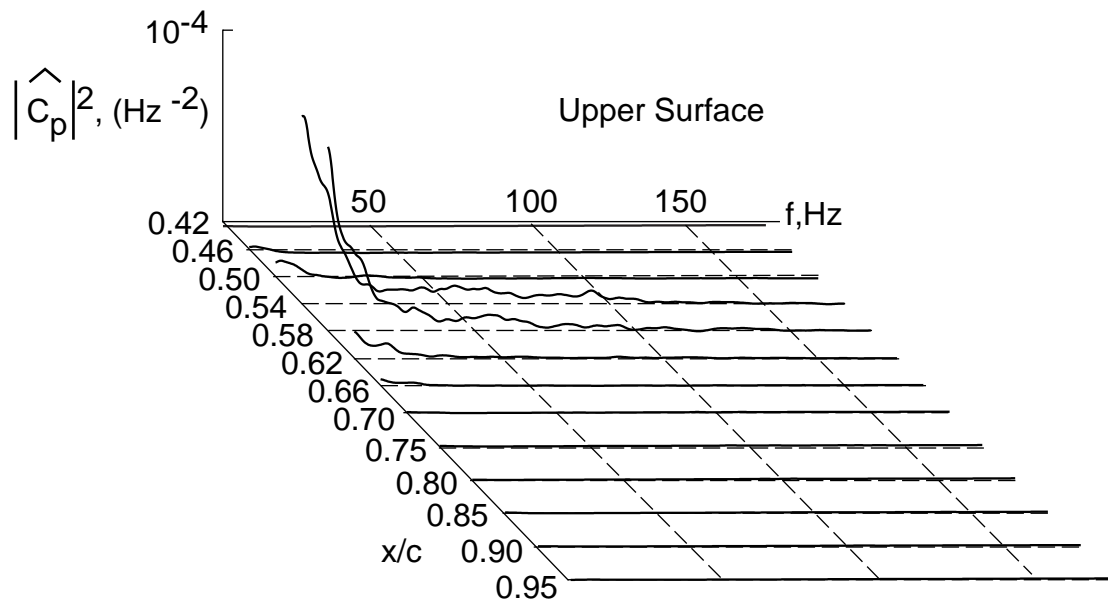


Figure 5. Chordwise distribution of unsteady airfoil pressure coefficient modulus squared, Case 2, $\text{Re} = 15 \times 10^6$.

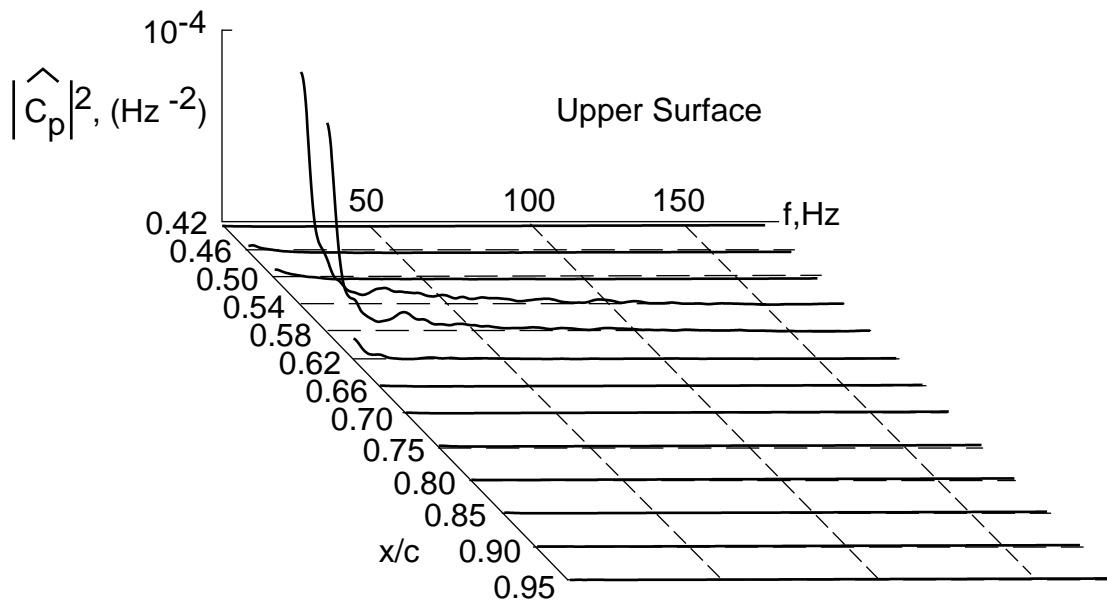


Figure 6. Chordwise distribution of unsteady airfoil pressure coefficient modulus squared, Case 3, $\text{Re} = 30 \times 10^6$.

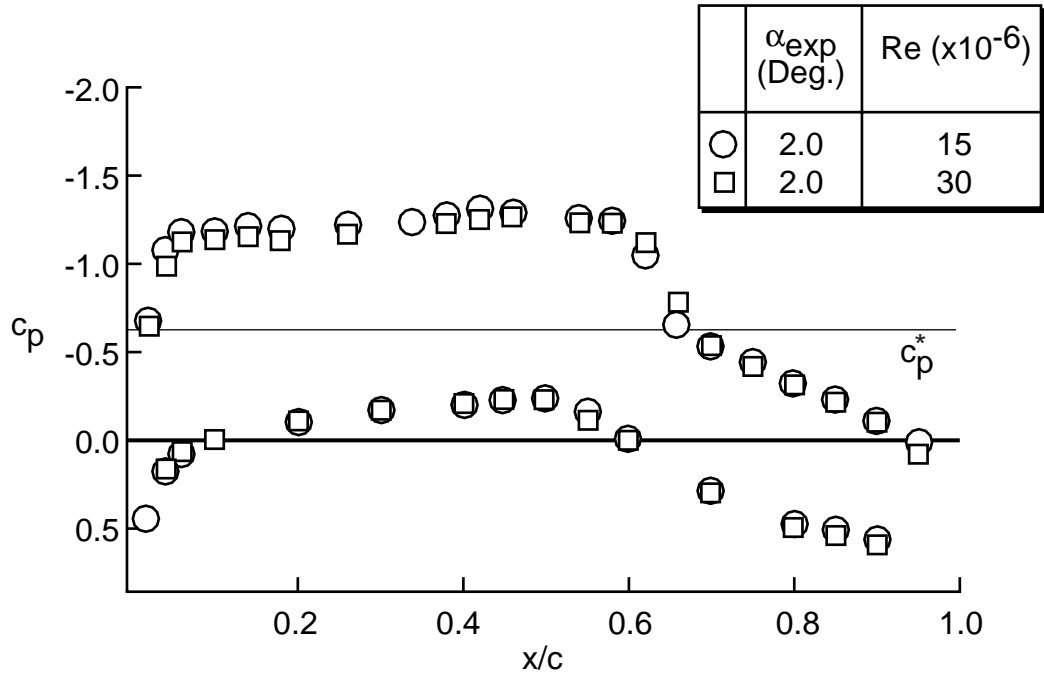


Figure 7. Chordwise distribution of mean pressure coefficient ,
Cases 4 and 6, $M_{exp} = 0.74$.

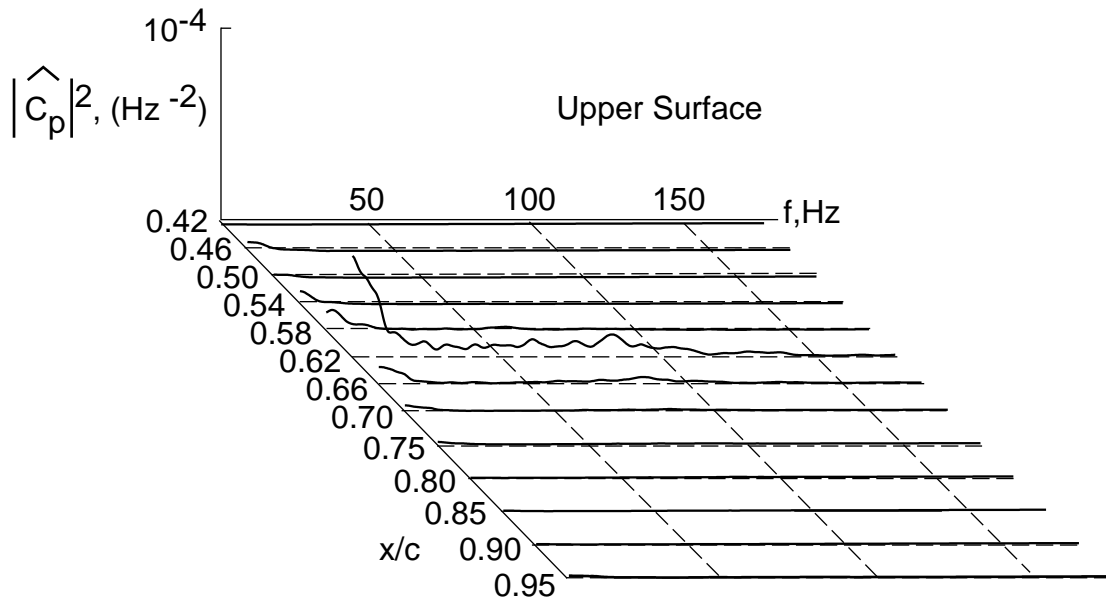


Figure 8. Chordwise distribution of unsteady airfoil pressure coefficient modulus squared,
Case 4, $Re = 15 \times 10^6$.

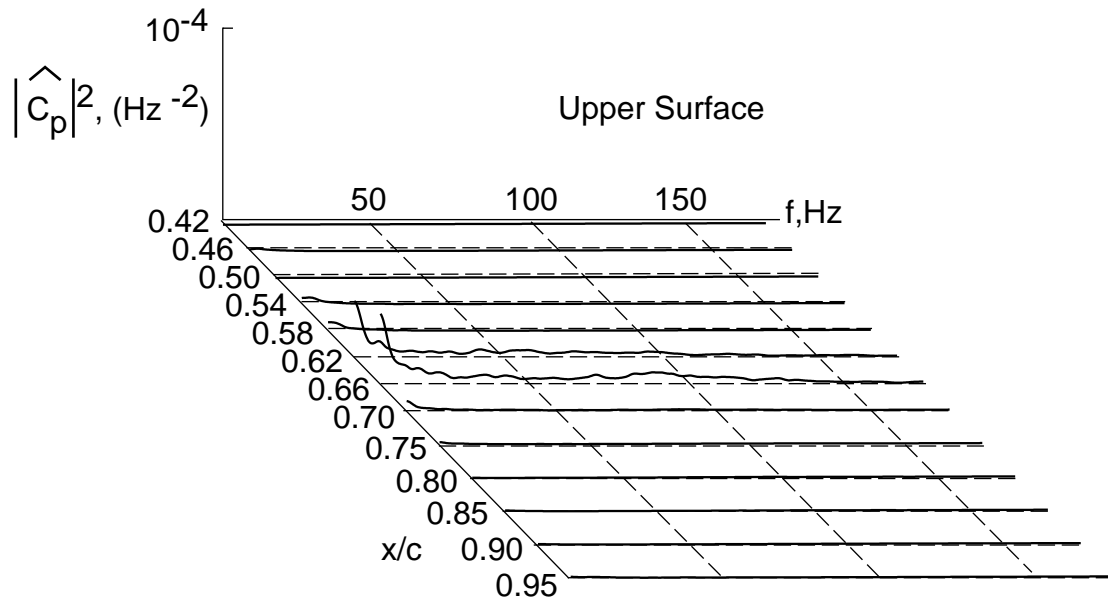


Figure 9. Chordwise distribution of unsteady airfoil pressure coefficient modulus squared, Case 6, $Re = 30 \times 10^6$.

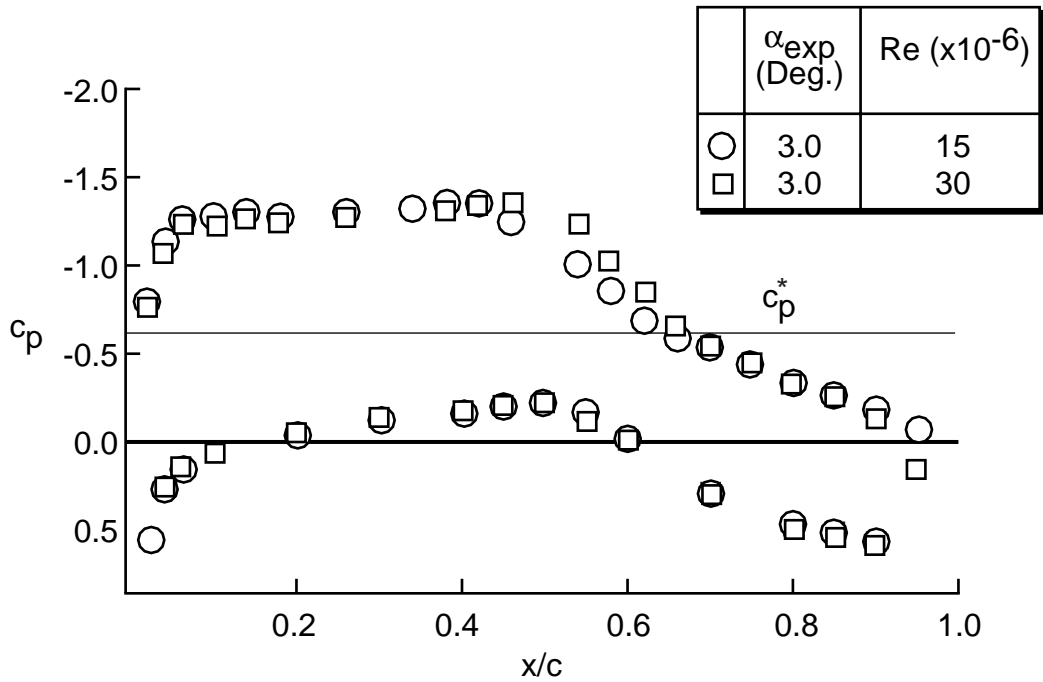


Figure 10. Chordwise distribution of mean pressure coefficient, Cases 5 and 7, $M_{exp} = 0.74$.

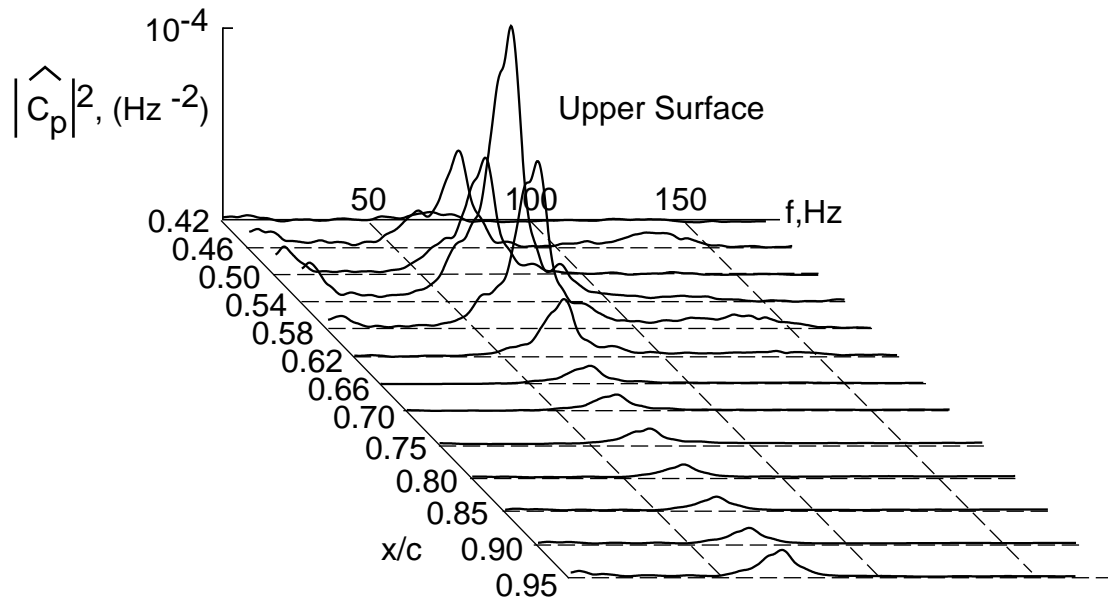


Figure 11. Chordwise distribution of unsteady airfoil pressure coefficient modulus squared, Case 5, $Re = 15 \times 10^6$.

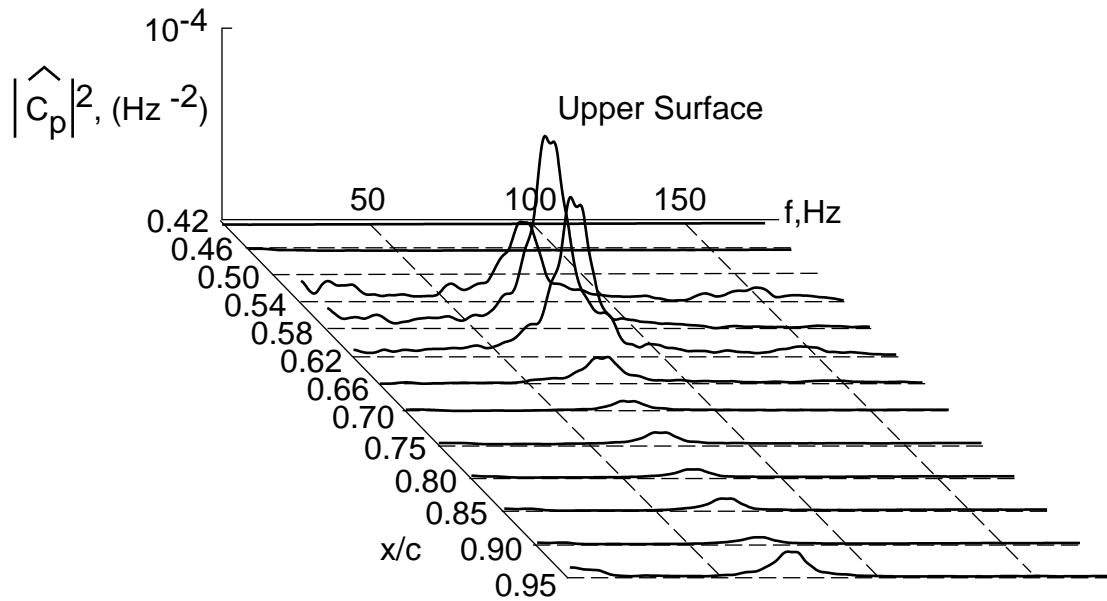


Figure 12. Chordwise distribution of unsteady airfoil pressure coefficient modulus squared, Case 7, $Re = 30 \times 10^6$.

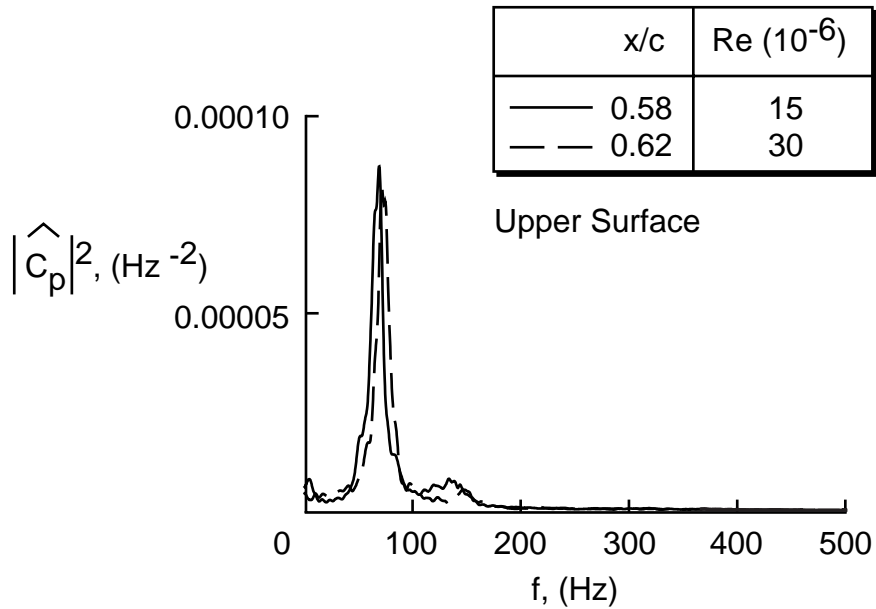


Figure 13. Shock buffet unsteady pressure coefficient modulus squared versus frequency, Cases 5 and 7.

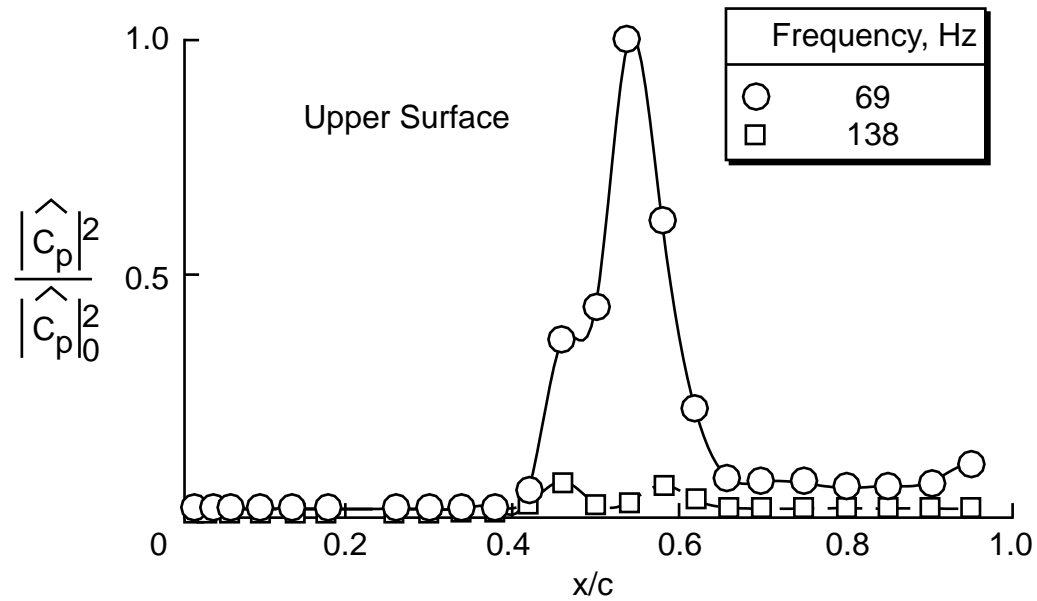


Figure 14. Shock buffet normalized unsteady pressure coefficient modulus squared versus chordwise location, Case 5, $Re = 15 \times 10^6$.